The Effect of Large Slice Thickness and Spacing and Low Coverage on the Accuracy of Susceptibility Mapping

Anita Karsa[1], Emma Biondetti[1], Shonit Punwani[2], and Karin Shmueli[1]

[1]*Medical Physics and Biomedical Engineering, University College London, London, United Kingdom,* [2]*Centre for Medical Imaging, University College London, London, United Kingdom*

Synopsis

Susceptibility Mapping has emerging clinical applications. To reduce scan time, clinical images are often acquired with large slice spacing/thickness and reduced coverage. The effect of these factors on susceptibility maps has not been investigated. Here, we develop a simple framework to explore the effect of low-resolution and low-coverage in the slice dimension on the accuracy of susceptibility maps. Our experiments with digital phantoms and volunteer images have shown that the error in the estimated susceptibility increases substantially with increasing slice spacing/thickness and decreasing coverage. These results underscore the need for high-resolution, full-coverage acquisitions for accurate susceptibility mapping.

Purpose

Magnetic Susceptibility Mapping (SM) is an emerging technique to reveal disease-related changes in tissue iron, myelin and calcium content and venous oxygenation[1]. Therefore, SM shows promise for several clinical applications[2] including Multiple Sclerosis[3–5], Parkinson's[6–8] and Huntington's[9] diseases. To reduce scan times and increase patient throughput, clinical images are often acquired with large slice spacing and slice thickness and reduced coverage in the through-slice dimension[3,8,10]. To accelerate translation of SM into the clinic, it is necessary to investigate the effect of these factors on the accuracy of SM. Others have probed the effect of a slightly increased slice thickness on susceptibility maps[11] but a comprehensive study of all these factors is needed. Here, we develop a simple simulation framework to investigate the effect of low slice resolution and low coverage of MR phase images on the accuracy of SM.

Methods

Simulations were performed on both numerical phantoms (with a matrix size of $256\times256\times256$) (Fig 1a), and 3D gradient-echo MR images acquired in a healthy volunteer (on a 3-Tesla Philips Achieva scanner, using a 32-channel head coil, SENSE factor = 2, with a matrix size of $240\times240\times144$, TE = 17.5 ms and TR = 49.54 ms, α = 10°) (Fig. 1b) both with initial 1 mm isotropic resolution. Numerical phantoms were generated to simulate spherical susceptibility sources of varying diameter (d) and susceptibility (χ) relative to their surroundings (Fig 1a). A phase map was calculated from the spherical phantoms at 3 T and TE = 12 ms using a Fourier-based forward model[12].

The raw brain phase image was unwrapped and the background field contributions were removed using the Laplacian technique[13] ($\sigma = 0.05$, two erosions of the FSL BET brain mask). The simulation pipeline in Figure 2a was then applied to both phantom and processed brain phase images:

1. The images were resampled in the z-direction to simulate either:
- increasing slice spacing by including only every k^{th} slice (Fig. 2b),
- increasing slice thickness by averaging the complex data across each slab of k slices in the z direction (Fig. 2c),
- low coverage by including the central n slices (Fig. 2d).

2. These low-resolution images were apodised in the slice dimension with a Planck-taper window function and zero padded up to the original matrix size for the phantoms and up to a matrix size of $512\times512\times256$ for the volunteer data.

3. Susceptibility maps were calculated using truncated k-space division[14] with a threshold of $\delta = 2/3$ and correction for underestimation of susceptibility values[13]. The kernel was set to zero at the centre of k-space.

4. The resulting susceptibility maps were compared with the ground truth susceptibility map for the phantoms and the full 'reference' susceptibility map obtained by processing the full phase image at full resolution and then extracting every k^{th} slice or the central n slices for both the phantoms and the volunteer

data. The root mean squared error (RMSE, Fig. 2a) of susceptibility in several regions of interest (ROIs, Fig. 1) was used to quantify the differences between the low-resolution/low-coverage and reference susceptibility maps.

Results and Discussion

The results of the simulations using phantoms are summarised in Figure 3. Here, the resulting susceptibility maps were compared with the full 'reference' map. Large slice spacing/thickness and low coverage induce a substantial error in the calculated susceptibility map (e.g. in Fig 3a, maximum RMSE = 86% of $\Delta\chi$). RMSE increases more rapidly with increasing slice spacing/thickness for smaller ROIs (Fig 3 a,b) and objects with higher susceptibility relative to their surroundings (Fig 3 d,e), while larger ROIs and regions with higher susceptibility are more sensitive to decreasing coverage (Fig 3 c,f). The results for the volunteer (Fig 4) show similar behaviour. Note the increased blurring and decreased contrast (Fig. 4d, red arrows) with increasing slice spacing. Calculated susceptibility maps of the phantoms were also compared with the ground truth susceptibility maps (Fig 5). The RMSE values have similar tendencies to those in Figure 3. The unexpected decrease in error around $*$ in Fig 5 is caused by the initial small overestimation of the susceptibility values by the correction technique[13].

Conclusions

Using a simple simulation framework, we have shown that increasing slice spacing/thickness and decreasing coverage reduce the accuracy of susceptibility maps. Smaller susceptibility sources and sources with a large susceptibility relative to their surroundings (e.g. red nuclei in Fig 4 a,b) suffer from larger errors in their susceptibility values at low resolution while larger regions are more sensitive to decreased coverage. These results underscore the need for high-resolution, full-coverage acquisitions for accurate susceptibility mapping. Future work may explore potential correction techniques.

Acknowledgements

This work was supported by the Engineering and Physical Sciences Research Council (EPSRC).

References

1. E M Haacke, S Liu, S Buch, W Zheng, D, Wu and Y Ye. Quantitative susceptibility mapping: current status and future directions. MRM. 2014

2. J R Reichenbach, F Schweser, B Serres and A Deistung. Quantitative susceptibility mapping: concepts and applications. Clinical neuroradiology. 2015

3. C Langkammer, T Liu, M Khalil, C Enzinger, M Jehna, S Fuchs, F Fazekas, Y Wang and S Ropele. Quantitative Susceptibility Mapping in Multiple Sclerosis. Radiology. 2013

4. C Wisnieff, S Ramanan, J Olesik, S Gauthier, Y Wang and D Pitt. Quantitative susceptibility mapping (QSM) of white matter multiple sclerosis lesions: Interpreting positive susceptibility and the presence of iron. MRM. 2015

5. X Li, D M Harrison, H Liu, C K Jones, J Oh, P A Calabresi and P C M van Zijl. Magnetic susceptibility contrast variations in multiple sclerosis lesions. J. Magn. Reson. Imaging. 2015

6. G Du, T Liu, M M Lewis, L Kong, Y, Wang, J Connor, R B Mailman and X Huang. Quantitative susceptibility mapping of the midbrain in Parkinson's disease. Mov Disord. 2015

7. N He, H Ling, B Ding, J Huang, Y Zhang, Z Zhang, C Liu, K Chen and F Yan. Region-specific disturbed iron distribution in early idiopathic Parkinson's disease measured by quantitative susceptibility mapping. Human Brain Mapping. 2015

8. J H O Barbosa, A C Santos, V Tumas, M Liu, W Zheng, E M Haacke and C E G Salmon. Quantifying brain iron deposition in patients with Parkinson's disease using quantitative susceptibility mapping, R2 and R2*. Magnetic Resonance Imaging. 2015

9. D JF Domínguez, A C Ng, G Poudel, J C Stout, A Churchyard, P Chua, G F Egan and N Georgiou-Karistianis. Iron accumulation in the basal ganglia in Huntington's disease: cross-sectional data from the IMAGE-HD study. J Neurol Neurosurg Psychiatry. 2015

10. C Tudisca, D Price, M Forster, H Fitzke and S Punwani. Exploration of change of T2* of metastatic and normal cervical lymph nodes caused by 100% oxygen breathing. Proc. Intl. Soc. MRM, 2014

11. W Li, C Liu and B Wu. Quantitative Susceptibility Mapping: Pulse Sequence Considerations. 2nd International Workshop on MRI Phase Contrast and QSM, Cornell University, Ithaca, NY, USA. 2013

12. J P Marques and R Bowtell. Application of a Fourier-based method for rapid calculation of field inhomogeneity due to spatial variation of magnetic susceptibility. Concepts Magn. Reson. B, 2005

13. F Schweser, A Deistung, K Sommer and J R Reichenbach. Toward Online Reconstruction of Quantitative Susceptibility Maps: Superfast Dipole Inversion. MRM, 2013

14. K Shmueli, J A de Zwart, P van Gelderen, T-Q Li, S J Dodd and J H Duyn. Magnetic Susceptibility Mapping of Brain Tissue In Vivo Using MRI Phase Data. MRM, 2009

Figures

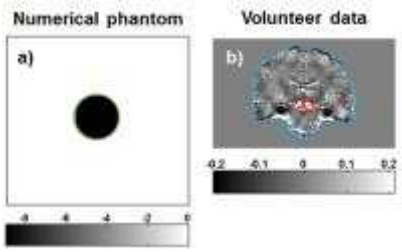

Figure 1: Numerical phantom of varying diameter and susceptibility (a) and full brain susceptibility map (b) in ppm showing ROIs: a) sphere (green) b) whole image, brain (blue) - mask obtained using FSL BET on magnitude image, red nuclei and substantia nigra (red) - ROI drawn manually on magnitude image.

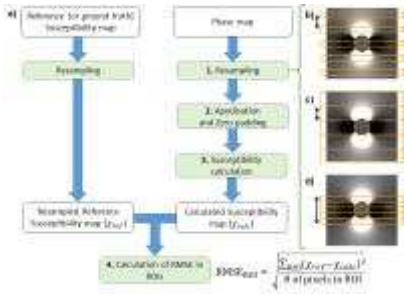

Figure 2: Framework (a) applied to the phantom and processed brain phase images. On the right side, the three different resampling methods simulating an increased slice spacing (b), increased slice thickness (c) and decreased coverage (d) are shown.

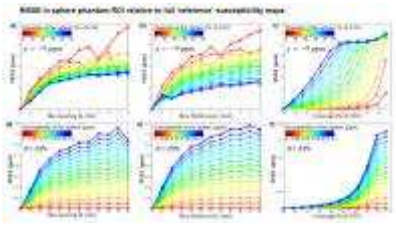

Figure 3: Effect of large slice spacing (a,d), thickness (b,e) and low coverage (c,f) (note the decreasing scale on the horizontal axis) on the RMSE in susceptibility maps calculated in spheres of varying size (a-c) and susceptibility (d-f). The calculated susceptibility maps were compared with the full 'reference' map.

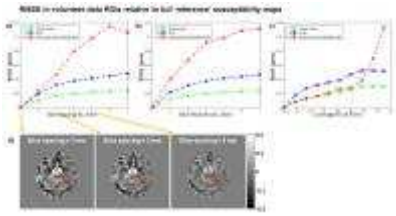

Figure 4: Effect of large slice spacing (a), thickness (b) and low coverage (c) (note the decreasing scale on the horizontal axis) on the RMSE in susceptibility maps of a healthy volunteer. Susceptibility maps calculated with different slice spacings are also shown (d).

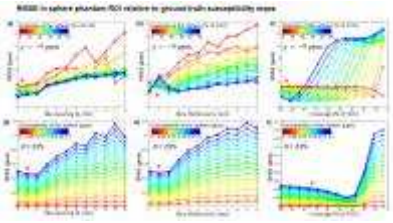

Figure 5: Effect of large slice spacing (a,d), thickness (b,e) and low coverage (c,f) (note the decreasing scale on the horizontal axis) on the RMSE in susceptibility maps calculated in spheres of varying size (a-c) and susceptibility (d-f). The calculated susceptibility maps were compared with ground truth susceptibility maps.

Proc. Intl. Soc. Mag. Reson. Med. 24 (2016)
1555